An Effective Multimodal Fusion of Ct and Mri Brain Images for Diagnosis of Alzheimer's Disease Using Waveatom

LEELA.M[1]*, DR.K. HELENPRABHA[2], DR.R. KARTHIK KRISHNA (MDRD)[3]

[1]*Research scholar, Anna University, Chennai*
[2]*Professor, Department of CSE, RMD Engineering College, Chennai*
[3]*Assistant Professor, Saveetha Medical College & Hospital, Chennai*
*Corresponding author: LEELA.M

Abstract

Medical image fusion technology is important for clinical use because it contains information from different types of images. Image fusion based on multiple types of medical images makes the quality of the merged images much better. Alzheimer's disease (AD) is a fatal brain disorder that has a devastating impact on memory and thinking. The prevention and treatment of AD are greatly aided by early diagnosis. By analyzing the functional and anatomical changes in the brain, and Alzheimer's disease diagnosis may be made using computers. Experts in the medical field still struggle to diagnose illnesses using a single modality due to a lack of data in this area. Different medical imaging systems may be fused using image fusion to provide a comprehensive image of a patient's health status, including the location and severity of any visible disorders. In this paper, we suggest a good way to combine the information from Computed Tomography (CT) and Magnetic Resonance Imaging (MRI) scans the image for the diagnosis of Alzheimer's disease. As a result, a medical image fusion strategy for multimodal MRI and CT images is provided in this study. For the fusion process, we proposed the Waveatom Transform approach. The suggested approach's performance is proven by fusing several sets of multimodal images and evaluating the suggested method's outcomes to the findings of certain other image fusion techniques. The performance metrics are compared with wavelet with CT image, wavelet with MRI image; wavelet with CT+MRI image, waveatom with CT image, waveatom with MRI image, and waveatom with CT+MRI image was analyzed. It has been discovered that the optimized strategy outperforms traditional fusion approaches in terms of performance.

Keywords: *Image fusion, Alzheimer's disease (AD), Waveatom Transform, Computed Tomography (CT), Magnetic Resonance Imaging (MRI)*

INTRODUCTION

The rapid advancement of computer technology has made medical imaging technology a crucial component of many therapeutic applications. Medical images with distinct modules display organ/tissue information from different imaging methods [1]. Clinicians use imaging techniques based on the situation. Multi-modal medical image fusion aims to fuse the source images with other modes that each carries a distinct kind of supplemental information to create a visual composite image that will aid clinicians in their diagnosis and decision-making. A neurodegenerative ailment called AD causes dementia and cognitive loss. By the year 2025, there will be 10 million AD sufferers living in the United States [2]. Automated computer-aided diagnostic techniques might thus significantly increase the efficiency of screening at-risk people. These procedures often use patient data as input, including, but not limited to, demographics, medical history, genetic sequencing, and images of the nervous system. The output is a diagnostic label that indicates the patient's health state and may also contain a probabilistic uncertainty about the prognosis. The lack of clarity around a clinical diagnosis of AD has sparked a hunt for imaging diagnostic indicators [3]. Numerous CT investigations have been conducted since the 1970s to look for signs of localized atrophy in AD patients' brains. Because AD patients were only diagnosed clinically, the overlap between AD and normal aging impeded the search. Atrophy affects both the ventricular and cortical systems. Normal axial CT scan angle obscures the medial temporal lobe [4]. Temporal horn dilation and suprasellar cistern enlargement imply medial temporal lobe alterations. They concluded that hippocampus atrophy is an early marker of deteriorating AD. Hippocampal atrophy is a typical AD neuroimaging finding. The axial temporal lobe-directed CT scan may examine for numerous infarcts, tumors, or hydrocephalus, and the temporal lobe-oriented scan (in 1.5-2 mm slices) can identify medial temporal lobe atrophy are indicated in figure 1.
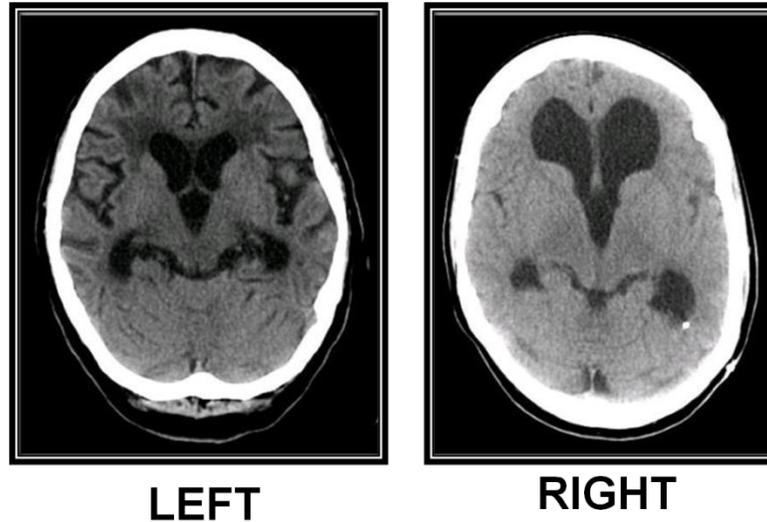
Figure 1: Left and right brain CT scan of an AD patient

A CT with AD is on the left, and a catheter is seen in sufferers with normotensive hydrocephalus (right). CT helps separate Alzheimer's disease from other brain illnesses. Unfortunately, the value of CT in the diagnosis of AD is relatively low. The availability of MRI has increased over the last 20 years, and it has subsequently been employed for the great majority of structural neuroimaging procedures [5, 21]. Alzheimer's disease is the most frequent cause of dementia. Neurofibrillary tangles (NFT) and beta-amyloid neuritic plaques are AD markers. AD brains had hyperphosphorylated tau. In this condition, normal tau's major functions are disturbed and paired helical filaments or NFTs polymerize, which causes synaptic loss. Overproduction of amyloid precursor protein causes high A42 levels and neuritic plaque development.
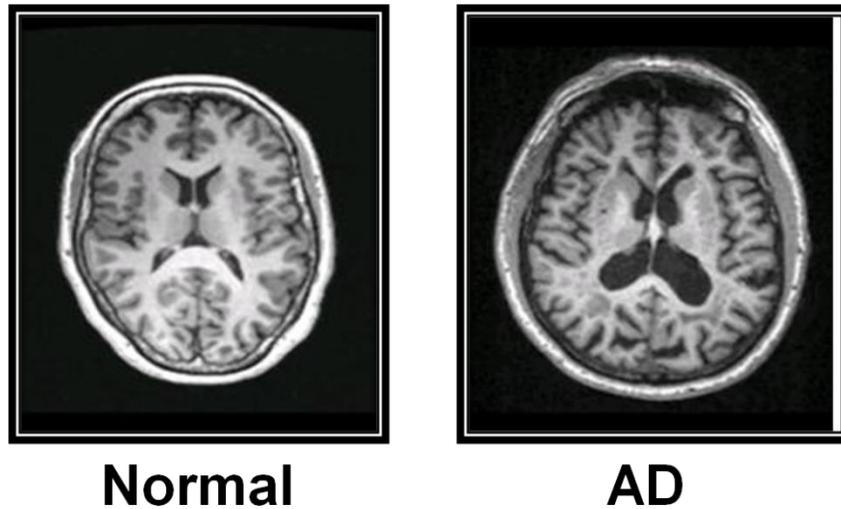
Figure 2: MRI scan image for normal and AD

This causes neuronal damage by oxidative and inflammatory stress. Atrophy initially appears in the entorhinal cortex (ERC) and hippocampus of the medial temporal lobe (MTL) [6]. AD patients have 26–27% smaller hippocampus and ERC sizes than controls. MCI causes moderate MTL atrophy [7]. AD patients with widespread hippocampus atrophy have an executive function and memory problems [8]. AD patients exhibit the highest losses in hippocampus volume compared to DLB and PDD. Feature space, transformational field, and deep learning are used in medical image fusion. The rapid rise indicates the need for computer-assisted clinical diagnostics. Different research advocated different fusion processes, each with its own set of benefits. 30 implementations exist for medical image fusion. Quantitative assessment markers for fusion effects vary. Indicator nonuniformity restricts request options. Medical image fusion research, although adequate, lacks novelty. The bulk of fusion techniques have been upgraded based on the initial methodologies; however, problems like chromatic warping and pattern information retrieval remain. Insufficient training data may lead to overfitting. Learning a complicated network takes time and needs several settings. Simplify the training system or enable simultaneous retraining. To address such problems, we proposed the Waveatom Transform approach. The suggested approach's performance is proven by fusing several sets of multimodal images and evaluating the suggested method's outcomes to the findings of certain other image fusion techniques.

Contributions of this research

❖ To use the median filter to minimize the influence of input noise values with exceptionally large magnitudes is one of the most significant advantages of the median filter in comparison to other filters.

❖ To assess the Kernel Principle Component Analysis (KPCA) identifies data patterns based on feature correlation. KPCA projects high-dimensional data into a new subspace with the same or less dimensions.

❖ One way offered to achieve this goal is the waveatom-based multifocus image fusion method.

The remainder part of this research is structured as Section 2- related work; Section 3- proposed work; Section 4- result and discussion; Section 5- conclusion.

RELATED WORKS

Here, we provide a summary of previous studies that are relevant to our strategy and application. Table 1 indicates the related works of this research.

Table 1: Related works of this research

Ref. no.	Author/ year	Description	Limitation
[9]	Li et al. (2020)	To generate supplementary, redundant, and low-frequency sub-band pictures, they use a Laplacian decision graph decomposition strategy with image augmentation. Considering the varied properties of redundant and complementary information, they present the overlapping domain (OD) and non-OD (NOD), where the OD fuses redundant information and the NOD fuses complimentary information	The lack of clarity around a clinical diagnosis of the medical image has sparked a hunt for imaging diagnostic indicators
[10]	Maqsood and Javed et al.	Introduces a multimodal image fusion approach that utilizes sparse representation and two-scale image decomposition. The suggested method initially	The disadvantage is that the learned dictionary cannot

	(2020)	applies a contrast enhancement approach to the source multimodal images, balancing out the intensity distribution for enhanced display.	adequately reflect the complicated input image structure.
[11]	Zhao et al. (2021)	For the practical requirements of medical diagnosis, a multi-mode medical image fusion with deep learning will be suggested.	Applied in batch mode for multi-modal medical image fusion, circumventing one-page processing constraint.
[12]	Zhu et al. (2019)	The unique strategy for fusing several medical imaging modalities based on phase congruency and local Laplacian energy.	Implemented in various multi-modal medical image fusion issues in batch processing mode, and may successfully overcome the constraint of just one-page processing.
[13]	Ganasala and Prasad et al. (2020)	New image fusion approach based on stationary wavelet transform (SWT) and texture energy measurements (TEMs) to solve fusion products' weak contrast and excessive processing cost. SWT pulls approximations and details from source images	A search for imaging diagnostic markers has been motivated by the lack of clarity around the clinical diagnosis of medical images.
[14]	Tao et al. (2018)	Using low-rank sparse component decomposition and dictionary learning, this research proposes a novel method for the fusion, denoising, and augmentation of medical images.	When images are corrupted by noise, the efficacy of fusion techniques diminishes drastically.

[15]	Xia et al. (2019)	Develop a novel multi-modal picture fusion method that employs multi-scale transformation and deep convolutional neural network features to improve medical diagnostic accuracy. In the first layer of the network, the Gauss-Laplace and Gaussian filters break the original images into numerous sub-images	The basis of this challenge is that it is difficult to adopt a fixed model to the fusion needs of a new fusion image, which makes acquiring previous knowledge challenging.
[16]	Dinh et al. (2021)	This study proposes two new methods to address the two issues. With the first method, low-frequency components are fused using the Equilibrium optimizer algorithm (EOA). The second approach uses the Prewitt compass operator to sum local energy functions to fuse high-frequency components.	A negative aspect of the merged image is the loss of fine detail.
[17]	Wang et al. (2018)	A new adaptive decomposition strategy is suggested to discriminate between high-frequency and low-frequency picture components to extract the smoothing layer and texture layer from the structural image.	Lack of clarity in clinical image diagnosis prompted the hunt for imaging diagnostic indicators.
[18]	Rajalingam et al. (2018)	To enhance the quality of fused multimodality medical images, this study developed a unique neuro-fuzzy hybrid approach.	The combined image lacks detail.
[19]	Peng et al. (2018)	This study presents a novel approach to image fusion by examining the usage of CNP systems to coordinate the merging of different types of medical images.	The choice of the high-frequency coefficients determines the low-frequency coefficient.

[20]		Analyze feature fusion's advantages and functionality. The fusion of two photos or numerous characteristics improves infection detection and categorization. Here, they explore medical researchers' methodologies.	Lack of clarity surrounding clinical image diagnosis has driven a quest for imaging diagnostic markers.

PROPOSED METHODOLOGY

Different medical imaging systems may be fused using image fusion to provide a comprehensive image of a patient's health status, including the location and severity of any visible disorders. In this study, we propose a useful method for combining the data from CT and MRI scan images for Alzheimer's disease diagnosis. As a consequence, this work offers a medical image fusion technique for multimodal MRI and CT images. Figure 3 indicates the proposed methodology of this research.
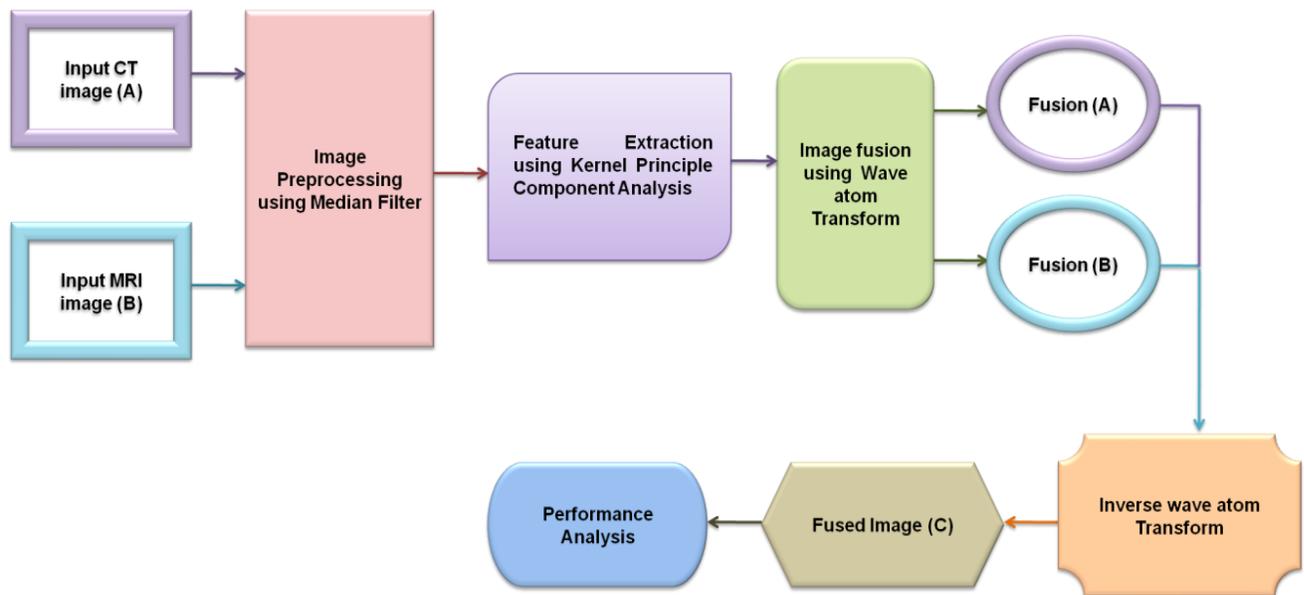
Figure 3: Proposed methodology of this research

A. Dataset

a. Input CT image (A)

This dataset on Alzheimer's disease was obtained from the Kaggle dataset. The URL for the dataset may be found here. "**https://www.kaggle.com/code/jeongwoopark/alzheimer-detection-and-classification-98-7-acc/data**"

b. Input MRI Image (B)

This dataset on Alzheimer's disease was obtained from the Kaggle dataset. The URL for the dataset may be found here. https://www.kaggle.com/code/davidebombassei/alzheimer-mri-model-group-7/data.

Figure 4 indicates the sample image for CT and MRI image, figure 4(a) indicates the CT image; figure (b) depicts the MRI image.

(a)   (b)
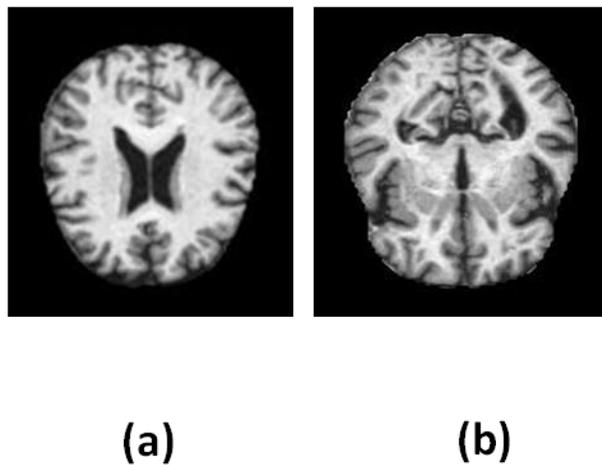
Figure 4: (a) CT image and (b) MRI image

B. Image preprocessing using Median Filter

To gain a competitive edge in the prior processes, image quality must always be enhanced. The image pre-processing plays a significant role in presenting the image's improved qualities. An effective adaptive median filter technique is utilized in this suggested system to improve the clarity of MRI and CT images on AD patients. This is a fairly effective method of removing impulse data from images. In the traditional median filter method, on the other hand, all of the

image's pixels are filtered equally, including both noisy and noiseless pixels. As a result, the pre-processed image will have faded corners, removed edges, and a blurred image. As a result, numerous varieties have been introduced. The factors aren't used explicitly by nonlinear filters. Their operation is based on the values of pixels in the area that is being considered. To remove grain noise from an image, apply an averaging filter. The median filter, on the other hand, can be used to reduce noise without distorting the image's crisp edges. It replaces a pixel with the median of all pixels in the surrounding area. Median filters are the most effective at reducing noise patterns with high spike-like components.

C. Feature Extraction using Kernel Principle Component Analysis (KPCA)

The KPCA algorithm is an extension of the principal components analysis (PCA) method that does not operate linearly. PCA works well with linear data and has limitations when trying to analyze nonlinear data. Images of people's brains must have some kind of nonlinear connection. Due to its ability to mine the nonlinear information in the dataset, KPCA provides additional benefits for identifying the major components and minimizing the dimension. The selection of the nonlinear mapping function ϕ is the decisive step in the KPCA analysis procedure. High-dimensional linear features (ϕ) are constructed from the input vector (Z). The PCA method is then used to analyze the data in the given space.

a. Nonlinear mapping function determination ϕ

It's common to practice using training samples in z= z_1, z_2,…z_q. A high-dimensional space, denoted by ϕ, is created from the training sample z. For the feature space to qualify, it must satisfy the following conditions:

$$\sum_{a=1}^{q} \phi(z_a) = 0, (i = 1,2 \dots q) \tag{1}$$

b. Estimating the covariance matrix $\widehat{T}$.

A description of the covariance matrix is given by

$$\bar{t} = \frac{1}{Q} \phi(z_a)\phi(z_a)^C \tag{2}$$

The high-dimensional spatial mapping makes it very challenging to solve analytically. Therefore, the covariance is often solved using the kernel function. Radial basis kernel functions are

examples of common kernel functions $S(z_a, z_d) = (g.k(z_a, z_d) + t).j$, polynomial kernel function $S(z_a, z_d) = (g.k(z_a, z_d) + t)^j$ and sigmoid kernel function $S(z_a, z_d) = tan \cdot l(m.kk(z_a, z_d) + o)$ etc. To define q*q matrix s $S_{yp} = \left(\phi(z_y).\phi\left(z_p\right)\right)$ $(y, p = 1, 2 \ldots \ldots q)$ can be calculated.

c. Localization of the Kernel Function Matrix.

Confirming that the centralized kernel function matrix N_q =N=A_qs -SA_q+ A_qs SA_q, A_q is a q*q matrix is necessary before can be determined. Further, each component is 1/q.

d. Evaluating eigenvalues and eigenvectors

The matrix N_q eigenvalues λ= (λ_1, λ_2, λ_x) and eigenvectors $\acute{\alpha}$= $\acute{\alpha}_1$, $\acute{\alpha}_2$, $\acute{\alpha}_x$ may be determined. Later, a fresh feature vector is derived using Schmidt's orthogonalization and unitization. The major component eigenvector β= (β_1, β_2, β_v… β_x) after features reduction computation is then found to be by computing the cumulative contribution rate. The KPCA technique is used to reduce data representation while preserving the most important features of a sample. Simultaneously, the dimension of the feature matrix is reduced by selecting the relevant eigenvectors based on the cumulative contribution rate, which in turn increases classification accuracy. KPCA offers two improvements over conventional PCA:

❖ First, we present a function for projecting data from their original low-dimensional space into a high-dimensional space.

❖ A theorem is stated which states that all space samples may be used to linearly represent any vector in space, including a basis vector.

D. Waveatom Transform

The waveatom transform was a newer mathematical transformation utilized in contemporary computational harmonic analysis. This transformation may adapt to different local orientations in a pattern, and it can also sparsely depict anisotropic patterns that are perpendicular to the axes. The mathematical definition of the parabolic scaling rule for the relationship between the duration of vibrations (i.e., frequency) of every wave atom and the size of vital support (i.e., circumference) is,

Wavelength $\acute{\alpha}$ diameter^2

Consider the following definition of the Fourier transform of a two-dimensional (2D) function, $\hat{n}(\omega)$, where $k = (k_1, k_2)$:

$$\hat{n}(\omega) = \int n(k)e^{-j\omega k}mk; \quad n(k) = \frac{1}{(2\pi)^2}\int \hat{n}(\omega)e^{j\omega k}m\omega \tag{3}$$

Let's define waveatoms as (k) with the subscript (q, h, r), where q denotes the resolution scale, h denotes the position in time ($[h_1, h_2]$, and r denotes the place in frequency ($[r_1, r_2]$). These five variables, which all have positive integer values and index the point (k_μ, ω_μ) in phase space, are q, h_1, h_2, r_1, and r_2, respectively.

$$k\mu = 2^{-q}h \text{ and } \omega_\mu = \pi 2^q r \tag{4}$$

With c1, c2 > 0 and 2^q a_1 max $|r_1, r_2|$ 2^q a_2. The wave vector designates the centers of bumps of $\hat{\varphi}_n^0(\omega)$ as, and the position vector, k, represents the center of (k).

$$\hat{\varphi}_s^0(\omega) = e^{-j\omega/2}\left[e^{ju_r}g(b_r(\omega - 2u_r)) + e^{-ju_r}g(b_{r+1}(\omega - 2u_r))\right] \tag{5}$$
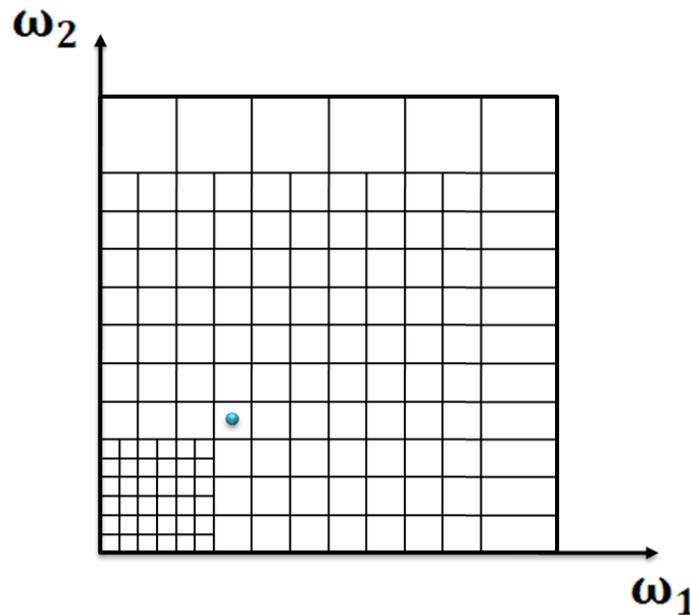
Figure 5: The frequency plane's wave atom tiling

The frequency plane's waveatom tiling is seen in figure 5. Fourier transforms of real-valued functions have a central symmetry around the origin, and may be understood if either $r_2 > 0$ or r_2

= 0 and $r_1 > 0$. When H is more than zero, the constituent parts of a wave packet frame are known as waveatoms.

$$\hat{\varphi}_n^0(\omega) = e^{-\frac{j\omega}{2}}[e^{ju_r}g(a_r(\omega - 2u_r)) + e^{-ju_r}g(a_{r+1}(\omega + 2u_r)) \tag{6}$$

The localization criteria have the following encoding for the parabolic scaling. The necessary frequency support at scale $\sim2^{-2k}$ is of size $\sim2^{-k}$ for each bump of $\hat{\varphi}_n^0(\omega)$, whereas the essential spatial support is of size $\sim2^{-k}$. Wavelength $\sim2^{-2k}$ characterizes the oscillations that take place within a waveatom's envelope in k.

a. Implementations 1D waveatoms

Tensor product of well selected 1D wave packets yields waveatoms. However, the inherent limitation of conventional wave packets is their inability to precisely localize frequencies. Using the equations $u_r = (-1)^r$ and $c^r = \frac{\pi}{2}(r + 1\ 2)$ Selecting g as a real-valued bump function on interval 2,

$$\sum_r |\hat{\varphi}_r^o(\omega)|^2 = 1 \tag{7}$$

Villemoes's design is notable because it allows for the creation of waveatoms with strong frequency localization through dyadic dilations and translations of $\hat{\varphi}_r^o$ on the frequency axis, i.e.

$$\varphi_{h,r}^q(k) = \varphi_r^q(k - 2^{-q}h) = 2^{q/2}\varphi_r^o(2^q k - h) \tag{8}$$

So, a function f is transformed into a series of waveatom coefficients by the waveatom transform:

$$c_{h,o}^k = \sum_{o=2\pi j} e^{j2^{-q}ho} \sum_{p\in 2\pi\mathbb{Z}} \overline{\varphi_r^q(o + 2^q p)}\, \hat{f}(o + 2^q p) \tag{9}$$

Waveatoms are seen here in their positive and negative forms:

$$\hat{\varphi}_{h,r}^q(\omega) = \hat{\varphi}_{h,r+}^q(\omega) + \hat{\varphi}_{h,r,-}^q(\omega) \tag{10}$$

Inverse Hilbert Function The solution to equation 6 is the orthonormal basis $L^2(S)$, denoted by $H\hat{\varphi}_{h,r}^q(\omega)$, which is produced via positive and negative bumps weighted linearly.

$$H\hat{\varphi}_{h,r}^q(\omega) = -j\hat{\varphi}_{h,r}^q + j\hat{\varphi}_{h,r-}^q(\omega)$$

b. Extension to 2D waveatoms

In terms of their 1D counterpart, 2D waveatoms may be defined in precisely three ways:

i.   Orthonormal basis

Individually obtaining tensor products of 1D waveatoms yields 2D orthonormal basis functions, i.e.

$$\varphi_\mu^+(k_1, k_2) = \varphi_{r_1}^q(k_1 - 2^{-q}h_1)\varphi_{r_2}^q(k_2 - 2^{-q}h_2) \tag{11}$$

Fourier transform expression:

$$\hat{\varphi}_\mu^+(\omega_1, \omega_2) = \hat{\varphi}_{r_1}^q(\omega_1)e^{-j2^{q_{h1k1}}}\hat{\varphi}_{r_2}^q(\omega_2)e^{-j2^{q_{h2,k2}}} \tag{12}$$

The Hilbert transform may be used to define a pair of orthonormal basis functions:

$$\hat{\varphi}_\mu^-(k_1, k_2) = H\varphi_{r_1}^q(k_1 - 2^{-q}h_1)H\varphi_{r_2}^q(k_2 - 2^{-q}h_2) \tag{13}$$

The frequency domain displays four lobes due to the oscillations occurring in two mutually perpendicular orientations.

ii.   Directional waveatoms

Orthonormal basis functions have the fundamental drawback of oscillating in two directions rather than just one, namely the k-direction. To address this issue, we may combine the fundamental (equation 11) with the dual (the Hilbert transformed basis) (Equation 13).

$$\varphi_\mu^{(1)} = \frac{\varphi_\mu^+ + \varphi_\mu^-}{2} \; and \varphi_\mu^2 = \frac{\varphi_\mu^+ - \varphi_{\mu\mu}^-}{2} \tag{14}$$

Builds a compact framework and supplies basis functions that are bi-lobed concerning the origin in the frequency domain, producing directional waveatoms. The redundancy of such a waveatom is increased by a factor of two to accommodate its unidirectional oscillation.

iii.   The complex waveatoms

This frequency domain symmetry breaking leads to subspaces of fixed k and n being exactly shifted invariant but at the cost of a factor of four more redundancy. However, neither orthonormal waveatoms nor directional waveatoms have the crucial characteristic of shift-

invariance. Since there is no overlap during the "wrapping" operation, aliasing is often eliminated when shift invariance is used. Because of its shift-invariant nature, complex waveatom is favored in the article above other 2D waveatoms for achieving fusion of images.

E. Fusion

Image enhancement is the use and interpretation of three-dimensional files of the body, typically collected from a Computed Tomography or Magnetic Resonance Imaging scanner, to detect disorders, direct medical treatments such as surgery preparations, or for investigation activities. The technique of merging numerous images within the same or other senses in terms of improving input images and conserving data is known as multi-modal medical image fusion. To conduct more thorough clinical investigations and make more accurate diagnoses of diseases, doctors often use the usage of medical image fusion. More specifically, complex waveatom, a version of the waveatom transform, exhibits a crucial characteristic that affects the efficacy of image fusion techniques, leading to the suggestion of waveatom transform-based medical image fusion.

F. Inverse Waveatom Transform

In inverse waveatom transform, the basic idea is to use the waveatom transform to deconstruct all input images and then fuse the resulting waveatom coefficients. The process of image fusion is carried out using higher clarity and crisper image sensitivities, inverse waveatom parameters are used. Lastly, the fused image is created using the inverse waveatom transform.

❖ The waveatom transform is initially used to break down the incoming multimodal medical images ά into levels.

❖ Because a greater intensity corresponds to a higher coefficient, the fused image's waveatom coefficients have the greatest values. Mathematically

$$W_Z^{R/1} = \begin{cases} W_k^{R/1} & if\ W_k^{R/1} > W_Y^{R/1} \\ W_Y^{R/1} & if\ W_k^{R/1} < W_Y^{R/1} \\ 0.5(W_k^{R/1} + W_Y^{R/1}) & if\ W_k^{R/1} = W_Y^{R/1} \end{cases} \tag{15}$$

Where $W_k^{R/1}$, $W_Y^{R/1}$, and $W_Z^{R/1}$ stand for the real (S)/imaginary (I) wave atom coefficients of images A, B, and the resulting image C, respectively.

❖ Create the final fused image by performing an inverse waveatom transform at the ά level (C).

RESULT AND DISCUSSION

The waveatom transform image fusion method's effectiveness is assessed using the following parameters: Peak Signal to Noise Ratio (PSNR), standard deviation, spatial frequency, and entropy. The performance metrics are compared with wavelet with CT image, wavelet with MRI image; wavelet with CT+MRI image, waveatom with CT image, waveatom with MRI image, and waveatom with CT+MRI image was analyzed. The existing methods such as Laplacian Pyramid-based Pulse Coupled Neural Network (LPPCNN), Hybrid medical image fusion using wavelet and curvelet transform (HW-CT), Non-subsampled complex wavelet transform (N-SCWT), and generative adversarial network (GAN) are compared with the proposed method to attain the greatest performance in this research. The performance metrics are compared with wavelet with CT image, wavelet with MRI image; wavelet with CT+MRI image, waveatom with CT image, waveatom with MRI image, and waveatom with CT+MRI image was analyzed. The CT image using wavelet transform are depicted in figure 6. Figure 7 illustrates the MRI image using wavelet transform. Figure 8 demonstrates that the original images to be wavelet fused image for CT and MRI images in AD.
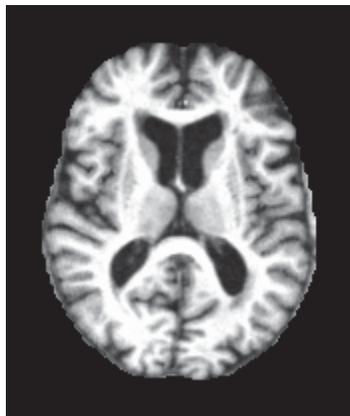
Figure 6: Wavelet with CT image
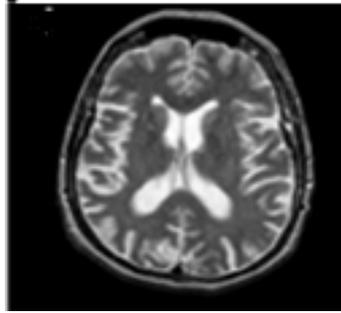
Figure 7: Wavelet with MRI image

Wavelet with
CT image

Wavelet with MRI
image

Wavelet with
CT+MRI image
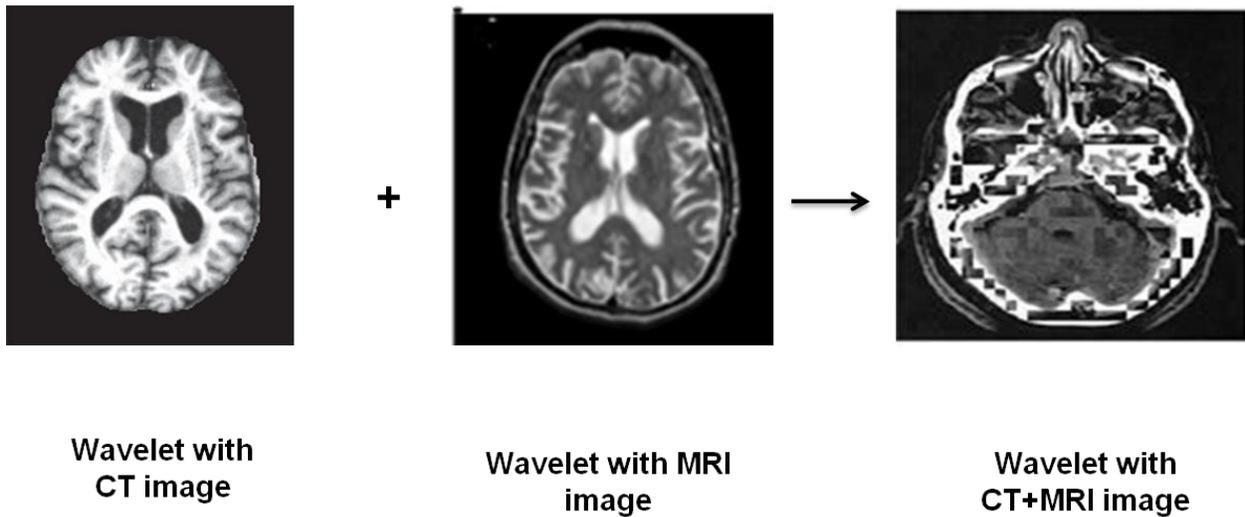
Figure 8: Wavelet with CT+MRI image

The MRI image is better at depicting soft tissues, whereas the CT image is better at depicting bones and hard tissues are illustrated in figure 9 and 10. According to figure 11, the results obtained using the waveatom transform fusing CT and MRI, the quality of the fused image improves with increasing levels of breakdown. By comparing the outcomes of the suggested fusion approach with those of various current state-of-the-art fusion methods based on, it is shown that the former is better.
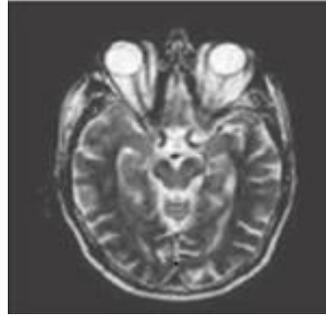
Figure 9: Waveatom with CT image
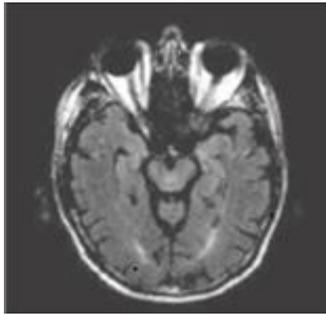
Figure 10: Waveatom with MRI image

Waveatom with
CT image

Waveatom with
MRI image

Waveatom with
CT+MRI image
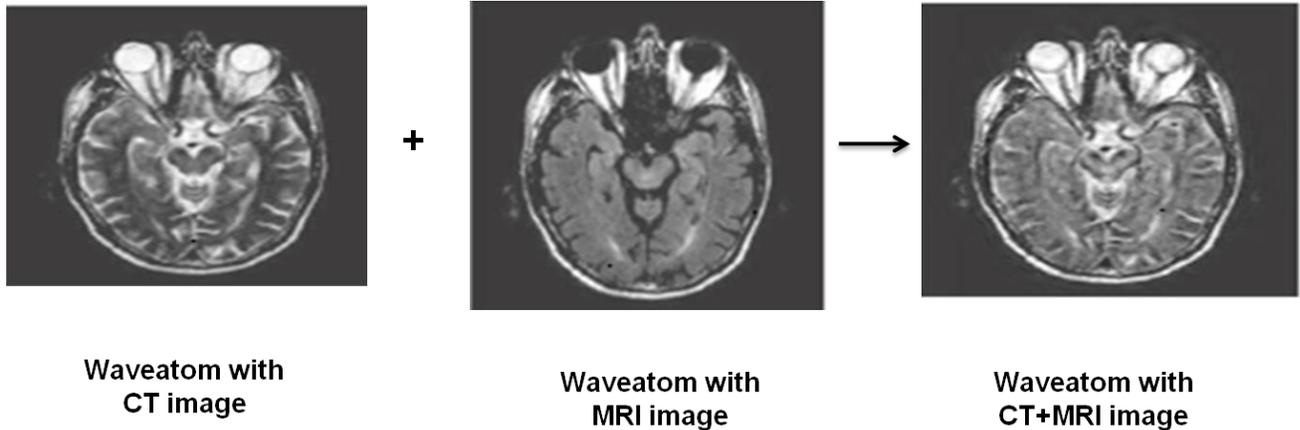
Figure 11: Waveatom with CT+MRI image

The spatial frequency of a structure is calculated as the number of times its oscillatory constituents (as measured by the Fourier transform) repeat per unit of distance. The spatial frequency is calculated in phases per pixel by the ratio $2\pi/N$. As shown in figure 12, the spatial frequency is higher in our proposed work than in the existing work. SD is made up of both input and distortion components, and it is effective in the lack of distortion. It assesses the level of

difference in the combined image. An image with a lot of difference will get a lot of SD. Figure 13 indicates the standard deviation of our proposed work.

$$\sigma^2 = \frac{1}{N-1} \sum_i^n (x - \mu)^2 \tag{16}$$

Where μ= number of pixels.

The quantity of dataset contained in an image is defined as entropy. Figure 14 indicates the entropy of the suggested work. Noise and other undesired fast fluctuations affect entropy. If the fused image's entropy is higher than the original image, it means the fused image has more datasets. The dataset substance of a fused image is calculated using the entropy.

$$He = -\sum_{i=0}^{L} h_{l_f}(i) log_2 h_{l_f}(i) \tag{17}$$

Figure 15 depicts the PSNR of our proposed work. When the fused and source images are identical, the PSNR will be below in our suggested approach. It's calculated as follows:

$$PSNR = 10 \, log_{10} \left(\frac{V^2}{RMSE} \right) \tag{18}$$

Where RMSE stands for Root Mean Square Error
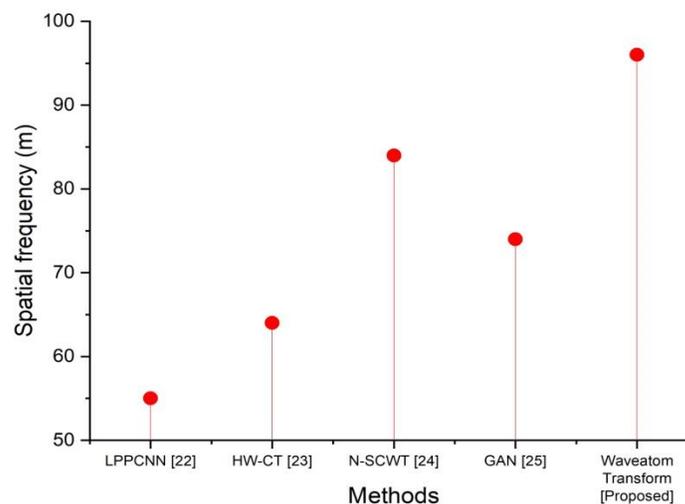
Figure 12: Spatial Frequency
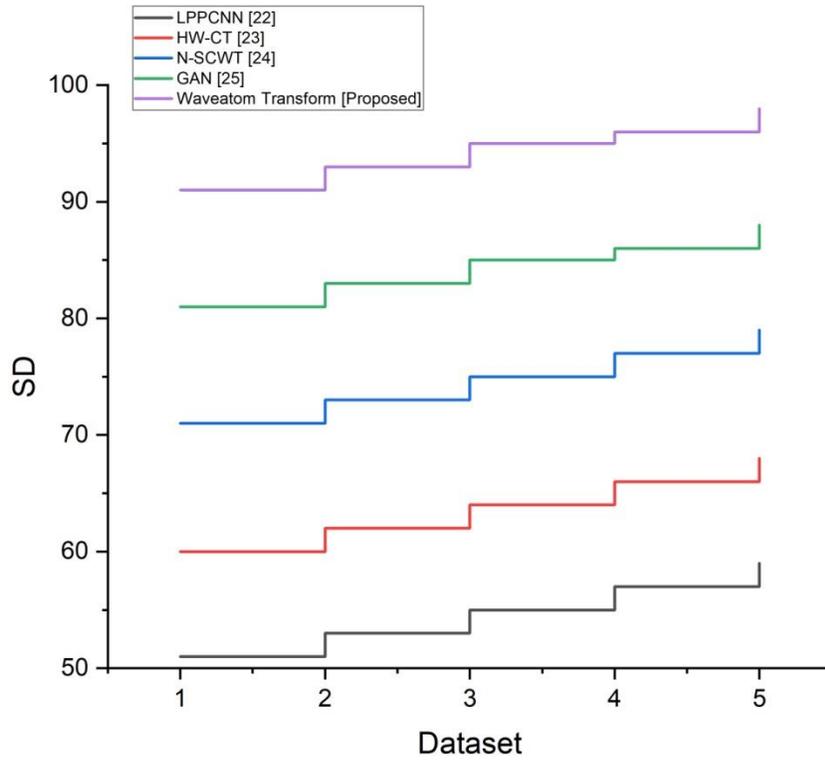
Figure 13: Standard Deviation
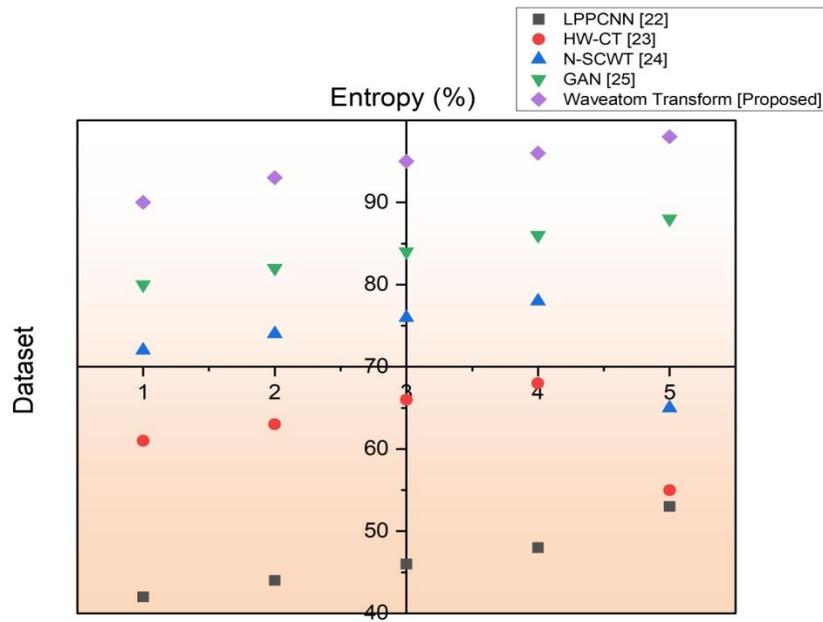
Figure 14: Entropy
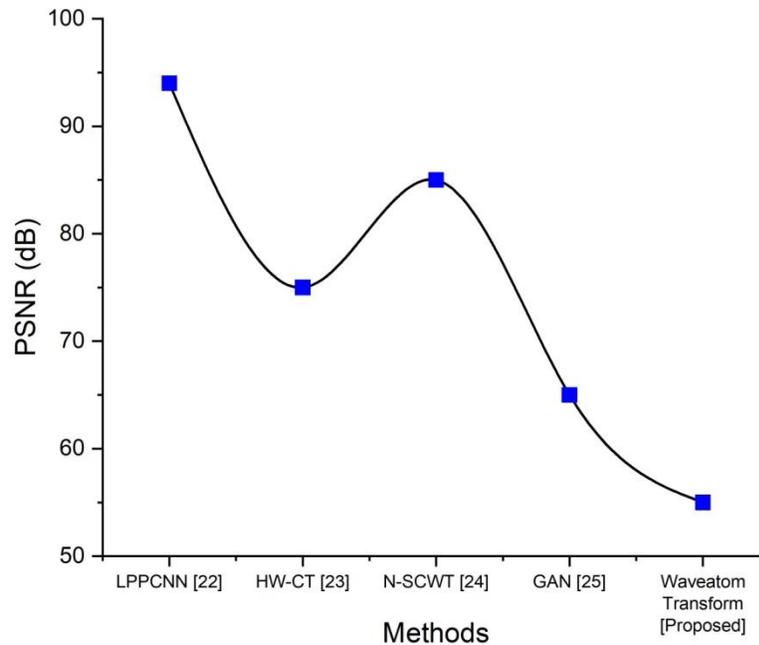
Figure 15: PSNR

Discussion

LPPCNN using multi-scale processing and adaptive selection are used to solve the artefact issue in the fusion results to improve the influence on human visual perception. Edges, textures, and other elements may be broken down into layers with various resolutions following various scales. Then, to create the fused pyramid, the matching layers of various source photos may be fused independently. Reconstruction is employed to create the combined image in the end. Medical image fusion has made extensive use of LP, yet this technology has an artefact issue (22). To address contrast restrictions and improve details in the fusion results, the HW-CT (existing) incorporates an additional enhancement phase employing adaptive and coupled adaptive histogram equalization and histogram matching (23). N-SCWT (existing) offers multiscale and multiresolution representation together with shift-invariance, phase information, and six-directional selectivity, all while reducing the computing cost (24). GAN (existing) are just migrations of other kinds of image fusion techniques, and such processes often result in the loss of elements that are inherent to the medical image itself (25). Because of the above problem, this paper attempts the fusion process by proposing the Waveatom Transform approach. The

suggested approach's performance is proven by fusing several sets of multimodal images and evaluating the suggested method's outcomes to the findings of certain other image fusion techniques.

CONCLUSION

This report introduces a medical image fusion procedure for multimodal MRI and CT images for AD brain images. We presented a Waveatom Transform based on the fusion process. The effectiveness of the suggested technique is demonstrated by fusing multiple types of multimodal images and evaluating the outcome to those of other image fusion methods. Spatial frequency, standard deviation, entropy, and PSNR can all be determined as a consequence. Finally, when compared to the other 4 existing works, the proposed work has high efficiency in terms of spatial frequency, standard deviation, and entropy. In the comparison graph, the PSNR of our suggested work is low when evaluated by the existing work, implying that the suggested technique is more efficient. When the waveatom transform on the dataset, it is discovered that the waveatom transform has a significant benefit in terms of de-noising the images, meaning that the recent research is capable of producing a high-quality fused image with more informative contents. As a result, the proposed work is quite useful and more efficient. The findings that were obtained by fusing CT and MRI using the waveatom transform showed that the quality of the fused image became better as the degrees of breakdown got higher. It has been established that the outcomes of the recommended fusion strategy are superior to those of a variety of existing state-of-the-art fusion approaches based on, and this has been accomplished by comparing the two sets of results.

There is a need for greater study to address the methodological constraints of more sophisticated modalities, which give unique insight into disease-specific patterns of neuropathology, even if only classic structural modalities are recommended for diagnosis in clinical practise of AD. This, we can only hope, will eventually lead to their incorporation into diagnostic criteria for AD. The fact that we've already used the planned waveatom transform is another constricting factor in our effort. We have also avoided CT scans and image fusion by just using MRI scans. As brain MRI pictures are often considered private, hospitals are reluctant to provide them for research purposes. We have tested the suggested model on a large dataset.

Reference

1. Hou, R., Zhou, D., Nie, R., Liu, D. and Ruan, X., 2019. Brain CT and MRI medical image fusion using convolutional neural networks and a dual-channel spiking cortical model. Medical & biological engineering & computing, 57(4), pp.887-900.

2. Alseelawi, N., Hazim, H.T. and Salim ALRikabi, H.T., 2022. A Novel Method of Multimodal Medical Image Fusion Based on Hybrid Approach of NSCT and DTCWT. International Journal of Online & Biomedical Engineering, 18(3).

3. Chang, L., Feng, X., Zhu, X., Zhang, R., He, R., and Xu, C., 2019. CT and MRI image fusion based on multiscale decomposition method and hybrid approach. IET Image Processing, 13(1), pp.83-88.

4. Tawfik, N., Elnemr, H.A., Fakhr, M., Dessouky, M.I., El-Samie, A. and Fathi, E., 2021. A survey study of multimodality medical image fusion methods. Multimedia Tools and Applications, 80(4), pp.6369-6396.

5. Adduru, V., Baum, S.A., Zhang, C., Helguera, M., Zand, R., Lichtenstein, M., Griessenauer, C.J. and Michael, A.M., 2020. A method to estimate brain volume from head CT images and application to detect brain atrophy in Alzheimer's disease. American Journal of Neuroradiology, 41(2), pp.224-230.

6. Marghalani, B.F. and Arif, M., 2019. Automatic classification of brain tumor and Alzheimer's disease in MRI. Procedia Computer Science, 163, pp.78-84.

7. Alongi, P., Sardina, D.S., Coppola, R., Scalisi, S., Puglisi, V., Arnone, A., Raimondo, G.D., Munerati, E., Alaimo, V., Midiri, F. and Russo, G., 2019. 18F-Florbetaben PET/CT to Assess Alzheimer's Disease: A New Analysis Method for Regional Amyloid Quantification. Journal of Neuroimaging, 29(3), pp.383-393.

8. Mehmood, A., Yang, S., Feng, Z., Wang, M., Ahmad, A.S., Khan, R., Maqsood, M., and Yaqub, M., 2021. A transfer learning approach for early diagnosis of Alzheimer's disease on MRI images. Neuroscience, 460, pp.43-52.

9. Li, X., Guo, X., Han, P., Wang, X., Li, H., and Luo, T., 2020. Laplacian redecomposition for multimodal medical image fusion. IEEE Transactions on Instrumentation and Measurement, 69(9), pp.6880-6890.

10. Maqsood, S. and Javed, U., 2020. Multi-modal medical image fusion based on two-scale image decomposition and sparse representation. Biomedical Signal Processing and Control, 57, p.101810.

11. Li, Y., Zhao, J., Lv, Z. and Li, J., 2021. Medical image fusion method by deep learning. International Journal of Cognitive Computing in Engineering, 2, pp.21-29.

12. Zhu, Z., Zheng, M., Qi, G., Wang, D., and Xiang, Y., 2019. A phase congruency and local Laplacian energy-based multi-modality medical image fusion method in the NSCT domain. IEEE Access, 7, pp.20811-20824.

13. Ganasala, P. and Prasad, A.D., 2020. Medical image fusion is based on laws of texture energy measures in the stationary wavelet transform domain. International Journal of Imaging Systems and Technology, 30(3), pp.544-557.

14. Li, H., He, X., Tao, D., Tang, Y. and Wang, R., 2018. Joint medical image fusion, denoising, and enhancement via discriminative low-rank sparse dictionaries learning. Pattern Recognition, 79, pp.130-146.

15. Xia, K.J., Yin, H.S. and Wang, J.Q., 2019. A novel improved deep convolutional neural network model for medical image fusion. Cluster Computing, 22(1), pp.1515-1527.

16. Dinh, P.H., 2021. Multi-modal medical image fusion based on equilibrium optimizer algorithm and local energy functions. Applied Intelligence, 51(11), pp.8416-8431.

17. Wang, J., Li, X., Zhang, Y., and Zhang, X., 2018. An adaptive decomposition method for multi-modal medical image fusion. IET Image Processing, 12(8), pp.1403-1412.

18. Rajalingam, B. and Priya, R., 2018. Hybrid multimodality medical image fusion technique for feature enhancement in medical diagnosis. International Journal of Engineering Science Invention, 2(Special issue), pp.52-60.

19. Li, B., Peng, H., Luo, X., Wang, J., Song, X., Pérez-Jiménez, M.J. and Riscos-Núñez, A., 2021. Medical image fusion method based on coupled neural P systems in the nonsubsampled shearlet transform domain. International Journal of Neural Systems, 31(01), p.2050050.

20. Khan, S.A., Khan, M.A., Song, O.Y. and Nazir, M., 2020. Medical imaging fusion techniques: a survey benchmark analysis, open challenges, and recommendations. Journal of Medical Imaging and Health Informatics, 10(11), pp.2523-2531.

21. Chandra, A., Dervenoulas, G. and Politis, M., 2019. Magnetic resonance imaging in Alzheimer's disease and mild cognitive impairment. Journal of neurology, 266(6), pp.1293-1302.

22. Si, Y., 2021. LPPCNN: A Laplacian Pyramid-based Pulse Coupled Neural Network Method for Medical Image Fusion. Journal of Applied Science and Engineering, 24(3), pp.299-305.

23. Sivakumar, N. and Helenprabha, K., 2017. Hybrid medical image fusion using wavelet and curvelet transform with multi-resolution processing. Biomedical Research (0970-938X), 28(6).

24. Talbar, S.N., Chavan, S.S. and Pawar, A., 2018, November. Non-subsampled complex wavelet transform-based medical image fusion. In Proceedings of the Future Technologies Conference (pp. 548-556). Springer, Cham.

25. Guo, K., Hu, X. and Li, X., 2022. MMFGAN: A novel multimodal brain medical image fusion based on the improvement of the generative adversarial network. *Multimedia Tools and Applications*, *81*(4), pp.5889-5927.